Density functional theory analysis of flexural modes, elastic constants, and corrugations in strained graphene

P. L. de Andres, F. Guinea, and M. I. Katsnelson

Donostia International Physics Center, Paseo Manuel de Lardizabal 4, 20018 Donostia, Spain,
Instituto de Ciencia de Materiales de Madrid (CSIC), Cantoblanco, 28049 Madrid, Spain, and
Radboud University Nijmegen, Institute for Molecules and Materials, Heyendaalseweg 135, 6525AJ NIjmegen, The Netherlands

Ab initio density functional theory has been used to analyze flexural modes, elastic constants, and atomic corrugations on single- and bi-layer graphene. Frequencies of flexural modes are sensitive to compressive stress; its variation under stress can be related to the anomalous thermal expansion via a simple model based in classical elasticity theory [P. L. de Andres, F. Guinea, and M. I. Katsnelson, Phys. Rev. B **86**, 144103 (2012)]. Under compression, flexural modes are responsible for a long-wavelength rippling with a large amplitude and a marked anharmonic behavior. This is compared with corrugations created by thermal fluctuations and the adsorption of a light impurity (hydrogen). Typical values for the later are in the sub-Angstrom regime, while maximum corrugations associated to bending modes quickly increase up to a few Angstroms under a compressive stress, due to the intrinsic instability of flexural modes.

PACS number(s): 63.22.Rc, 65.80.Ck, 61.48.Gh

I. INTRODUCTION

Physical properties of single and multilayered graphene are remarkable and open interesting avenues for applications in the future.[1] However, to realize their potential it is important to fully understand the elastic properties of graphene layers,[2] the effect of external stresses on electronic properties,[3,4] or conversely, the effect of doping on mechanical properties,[5] and the appearance of ripplings,[6,7] corrugations, and other defects expected under actual conditions of cleanness, temperature, and growth. The understanding of any departure from perfect two-dimensional (2D) configuration (e.g., rippling and corrugation) of very thin graphene layers, either in free suspension or deposited on a template substrate, is central for manufacturing processes.[8,9] At $T = 0$ K, in the absence of defects, the carbon bond on the graphene layer is well understood in terms of the formation of three in-plane localized strong sp^2 bonds, and a fourth delocalized, out-of-plane, π-like bond.[1,10] The optimum geometrical configuration is achieved by a honeycomb lattice formed by two equivalent sublattices displaying *P*6/*mmm* symmetry. The corresponding electronic structure shows bands dispersing linearly around the Fermi energy that are responsible for the fast and efficient transport of carriers. Both experimentally and theoretically,[2,11,12] it is shown that this kind of arrangement results in a material with the largest in-plane elastic constants known yet. Therefore the 2D perfect flat layer makes the most stable configuration, since deviations from a common plane require a significant amount of energy. Any departure from such a scenario affects greatly the atomic scale properties of the layer and must be understood in order to efficiently exploit graphene's properties. Different reasons, however, might be invoked for a two-dimensional graphene layer to adopt a certain corrugation at different scales. First, at a nonzero temperature there is a thermodynamic argument that implies the impossibility for a perfect 2D layer to exist in 3D.[6,10,13–16] Second, defects like adsorbed impurities, vacancies, etc., create local corrugations at the atomic scale[17] that propagate via the elastic properties of the lattice originating long-range correlations. Finally, external

applied stresses related to conditions on the boundary make graphene to bend and to corrugate, an interesting point to study since the growth of graphene layers on different supporting substrates implies mismatches that introduce all kinds of stresses that have been observed to originate a highly complex and corrugated landscape.[9,18] Research on these issues require atomically resolved techniques; theoretical simulations performed with *ab initio* density functional theory (DFT)[19,20] give an accurate picture of the interatomic interactions and can provide valuable information about geometry, vibrations, electronic effects, etc., down to the atomic level. Indeed, *ab initio* DFT has been successfully applied for many years now to describe the different allotropes of carbon, like graphite, diamond, fullerenes, organic molecules, nanotubes, etc. (e.g., see Refs. 11, 21, and 22). Here, we focus on the role of external stresses on the flexural modes ultimately responsible for the intrinsic thermodynamic instability of these layers. The frequencies of these modes are very sensitive to external compressive stresses and can be related, in turn, to the Grüneisen coefficients and the thermal expansion coefficient of graphene.[23] The purpose of this paper is to use state-of-the-art *ab initio* DFT to compare atomic corrugations on graphene layers related to three different origins: (i) the presence of small adsorbed impurities (hydrogen), (ii) thermal vibrational amplitudes ($T = 300$ K), and (iii) the long-wavelength corrugation characteristic of flexural modes. We analyze the consequences of an isotropic compressive stress on these corrugations, the elastic constants, and the phonons.

II. *AB INITIO* DENSITY FUNCTIONAL ATOMISTIC MODEL

Since we are interested in elastic and vibrational properties, we use accurate norm-conserving pseudopotentials to describe carbon valence-band electrons ($2s^2 2p^2$).[24,25] Electronic wave functions were expanded in a plane-wave basis set to an energy cutoff of 750 eV, and a $12 \times 12 \times 2$ Monkhorst-Pack mesh was used to sample wave functions inside the

first Brillouin zone. Electronic bands were obtained using a smearing width of $\eta = 0.1$ eV. The choice of the exchange and correlation (XC) potential opens up various possibilities. We favor the local density approximation (LDA)[26] because of its simplicity, excellent structural results for a wide range of carbon allotropes relevant for this work, and in particular, because even if somehow fortuitous, it predicts a reasonable value for the layer separation in graphite. LDA presents a solid record, reproducing many key features for a wide variety of carbonaceous materials, and it has been a standard choice in the literature for many authors. Unfortunately, the use of LDA cannot be justified *a priori* on physical grounds by merely referring to the behavior of the next term on a gradients expansion (GGA); different flavors of GGA yield worse agreement with experiments (e.g., for the distance between planes in graphite), showing that the converge on such an expansion is not a trivial one. Therefore we are forced to justify the use of LDA on the *a posteriori* reasonable structural results. Its simpler formulation should also be taken as an advantage, since it makes a better defined and more unique formulation. Finally, it is known that LDA may not be too accurate for absolute values of total energies, but it affords a good description of relative values (e.g., barriers) and it yields the correct dependence with stress after a single common offset correction.[27] A periodic supercell with a vacuum gap in the perpendicular direction (30 Å) and several $n \times m$ in-plane periodicities ($n, m = 1$–8), depending on the requirements of each model, were used. Geometrical parameters were optimized so residual maximum forces and stresses were kept below $F_{max} \leqslant 0.0001$ eV/Å, and $S_{max} \leqslant 0.0002$ GPa for the calculation of phonons and elastic constants, yielding a lattice parameter for the rhombohedral unit cell on a single graphene layer of $a = b = 2.447$ Å (Fig. 1) and $c = 6.65$ Å for graphite (Bernal stacking). Calculations were performed with the CASTEP code, as implemented at Materials Studio.[28,29]

The elastic tensor was obtained by applying a series of strains on the 1×1 unit cell (maximum amplitude 0.003 Å) and by computing the associated stress tensors.[30] Phonons were computed using linear response theory.[31] As a global benchmark to the elements included in our calculations (pseudopotential, exchange and correlation model, different

TABLE I. Comparison of *ab initio* elastic constants (GPa) computed for graphite with experimental values determined on single crystals by inelastic x-ray scattering (Ref. 33), on highly oriented pyrolitic graphite (HOPG, Ref. 32), and independent theoretical calculations.[34]

	c_{11}	c_{12}	c_{13}	c_{33}	c_{44}
X-ray scattering					
(Ref. 33)	1109 ± 16	139 ± 36	0 ± 3	39 ± 7	5 ± 3
HOPG (Ref. 32)	1060 ± 20	180 ± 20	1.5 ± 0.5	37 ± 1	0.3
Independent Calc.					
(Ref. 34)	1109	175	-2.5	29	4.5
This work	1069	204	-2.8	32	1

convergence thresholds, etc.), we compare in Table I our theoretical results for the five independent components of the elastic tensor for graphite to experimental values measured on pyrolitic graphite by ultrasonic resonance,[32] and on single crystals by inelastic x-ray scattering.[33] A comparison to a recent independent theoretical determination has also been included.[34] The agreement is quite reasonable, except perhaps for c_{13} that cannot be described properly with a local choice for exchange and correlation. We notice that the basal in-plane theoretical Poisson ratio, $v_{xy} = v_{yx} = \frac{c_{12}}{c_{11}} = 0.19$, and the Young modulus, $Y_x = Y_y = 1$ (TPa), are in good agreement with experimental values, 0.165 and 1.1 TPa, respectively;[32] as expected, these are very similar for a graphene monolayer (0.18 for theory to be compared with a quoted experimental value of 0.17, Ref. 2).

Values for the 2D elastic constants of a single graphene layer (I),[35] the bilayer with the usual AB Bernal stacking, and a bilayer with direct AA stacking (distance between layers 3.5 Å) display little variation in the main elements of the elastic tensor (see Table II; for reference, 2D tensions for graphite are quoted). The main departure was found for the AA bilayer in the *metastable* configuration (distance between layers 1.5 Å);[3] the reduction of c_{11} is related to the gradual transformation of the in-plane C-C bond order from sp[2] towards sp^3, since the 2D unit cell needs to be expanded to make the structure metastable under its own pressure. The increase in c_{66} implies
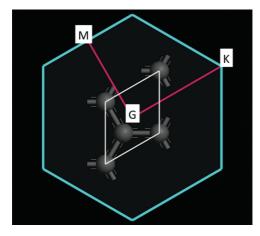

FIG. 1. (Color online) Graphene rhombohedral 1×1 unit cell ($\gamma = 60$) and corresponding Brillouin zone. (Special points are labeled according to the phonon calculation in Fig. 2.)

TABLE II. Elastic constants (eV/Å^2) normalized to the carbon mass in the 1×1 graphene unit cell. Results are given for (I) a single graphene layer, (AB) bilayer with Bernal stacking, (AA) bilayer with direct stacking, (AA') metastable bilayer at short distances (Ref. 3), (Bulk) graphite, and experimental values for graphite (Exp., Ref. 52). DFT calculations have been performed using LDA and norm-conserving pseudopotentials as explained in the text. No attempt to compute elastic constants involving strains in the z direction has been made for supercells with a vacuum separator.

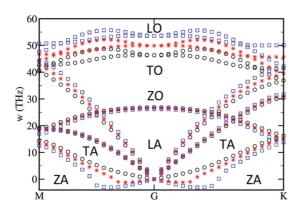| c_{ij}	I	AB	AA	AA'	Bulk	Exp.
c_{11}	23	22	22	11	22	22
c_{12}	4	4	4	4	4	4
c_{66}	9	9	9	3	9	9
c_{33}					0.25	0.28
c_{44}					0.01	0.03
c_{13}					-0.1	0.1

FIG. 2. (Color online) Phonons for the freestanding graphene layer (THz). Path: $M(0, \frac{1}{2}, 0) \rightarrow G(0,0,0) \rightarrow K(\frac{1}{3}, \frac{2}{3}, 0)$. Black circles: $\epsilon = 0$. Red stars: $\epsilon = -0.02$. Blue squares: $\epsilon = -0.04$.

a larger tendency against shear due to substitution of the weak van der Waals-like interaction between both layers by stronger sp^3-like chemical bonds.

For the two-dimensional graphene layer, due to its sixfold symmetry, we need to determine only two independent values in the elastic tensor. These can be related to the two Lamé coefficients needed to characterize an isotropic system: $\lambda = c_{12}$ and $\mu = c_{66}$. An independent determination of c_{11}, that should be equal to $c_{12} + 2c_{66}$, holds fairly well in all the cases. Therefore simple analytical models based in the theory of elasticity that need values for only these two parameters make a good approximation and can be thoroughly analyzed.[23,36] Under a moderate compressive stress (e.g., $\epsilon = -0.04$) the main change happens in the value of c_{12} that is reduced by ≈ 2.

Figure 2 gives the phonons for graphene along two main directions in the irreducible part of the Brillouin zone: G-M and G-K (Fig. 1). Since there are two atoms in the unit cell, we find three acoustic (ZA, TA, and LA) and three optical modes (ZO, TO, and LO). The optimized structure shows a computed vibrational spectra that agree well with previous calculations in the literature,[37] as can be seen by comparing frequencies for the modes at selected high-symmetry points (Table III). For $\epsilon = 0$ (no external stress, black circles), all the frequencies are positive and behave as expected; it is interesting to observe how the lowest acoustic mode (ZA) disperses quadratically, a characteristic feature for a 2D system [e.g., see Eq. (3) in Ref. 23].

A. Instability of flexural modes under compression

The intrinsic instability of the layer against compressive strain is demonstrated by the appearance of negative frequencies in a small region around the G point; the ZA phonon softens and goes to negative values.[38,39] It is worth noticing

TABLE III. Comparison of selected phonon frequencies (THz) at high-symmetry points in the Brillouin zone.

	G	M							K			
Saito *et al.*[37]	49	27	47	43	39	24	20	14	45	39	32	18
This work	48	27	44	41	40	20	19	14	42	37	31	16

that because of the extreme asymmetry between compression and tension for strain-induced instabilities on graphene layers, we have only considered compressive strains.[39] Other failure mechanisms for graphene under tension have been studied elsewhere.[40] For some critical wave vector $q = q_c$, the mode becomes again positive and the value of q_c increases with the amount of stress. The value of q_c defines a characteristic wavelength, $\lambda_c = \frac{2\pi}{q_c}$, with an amplitude that depends directly on the strain. This lowering of the frequency of the ZA modes under compression is consistent with the negative Grüneisen coefficients reported in the literature.[11,23,41,42] A fit to the results in Fig. 2 gives $\omega_{\vec{q}}^2 (\text{THz}^2) \approx -25|\vec{q}|^2 + 112|\vec{q}|^4$ for $\epsilon = 0.02$ and $|\vec{q}|$ in Å^{-1} (valid near the center of the Brillouin zone). For a–2% strain the corresponding 2D stress tensor is $\sigma = \sigma_{xx} = \sigma_{yy} = 0.6$ eV/Å^2, $q_c \approx 0.35$ Å^{-1}, and $\lambda_c \approx 12$ Å. Another relevant feature under stress observed in Fig. 2 is the hardening of LO and TO modes by $\approx 20\%$ for $\epsilon = -0.04$. These modes correspond to displacements inside the plane of the layer, play an important role in the dissipation of energy after the absorption of electromagnetic radiation,[43,44] and are strictly degenerate at the G point.

Note, finally, that the softening of the ZA and ZO modes under strain, shown in Fig. 2, will enhance the intrinsic spin-orbit coupling of graphene.[45]

III. CORRUGATIONS UNDER STRESS

A. Flexural modes

We address the question of deformations related to the intrinsic instability brought by the flexural AZ mode. Under compressive strain, the negative region of frequencies near the G point indicates the existence of an energetically favorable deformation for the system. Therefore, we essay a cosinelike perturbation with a wavelength corresponding to q_c on a rectangular 8×2 supercell under a range of strains from–2% to–5%. These strains are large enough for the wavelength determined by the 8×2 supercell. It has been previously shown by Zhang and Liu[39] that wavelengths of periodic undulations scale inversely with the square root of strain, setting a minimum value for a given wavelength that is <1% for the 8×2, and is therefore compatible with the values we use here. For $\epsilon = -3\%$, the soft mode displayed in Fig. 3 allows the system to gain -26 meV with a maximum amplitude of
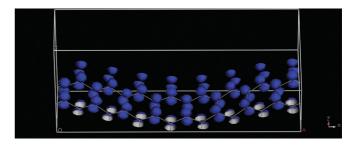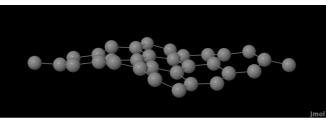

FIG. 3. (Color online) Long-wavelength deformation related to the AZ mode computed on a 8×2 rectangular unit cell ($\epsilon = -0.03$). Average and maximum corrugations are $\bar{c} = 0.66$ and $c_M = 2.03$ Å, respectively. The density of states at $E_F + 1$ V over the C atoms is shown (STM image in the Tersoff-Haman approximation).

$c_M = \max(z_i) - \min(z_j) = 2.03$ Å, and an averaged corrugation of $\bar{c} = \frac{1}{N}\sum_{i=1,N}|\bar{z} - z_i| = 0.66$ Å. Larger stresses drive the nonlinear behavior of the system. For $\epsilon = -5\%$ we find an energy gain of -3059 meV and $c_M = 2.81, \bar{c} = 0.92$ Å. It is interesting to notice that the density of states at the Fermi level (e.g., the Tersoff-Haman STM image) for such a long-range rippling of graphene is symmetric with respect to the two sublattices, as can be seen in Fig. 3, where the density of states has been drawn on each C atom for $V = 1$ V. Corrugations of this kind are expected to evolve smoothly into long-wavelength deformations in larger unit cells, unlike the case for thermal or defect-induced corrugations we study below.

B. Thermal fluctuations and light impurity adsorption

To quantitatively compare corrugations on graphene layers originated from other effects, we investigate the effect of thermal fluctuations ($T \neq 0$ K). The relationship between stresses originating in free finite edges and thermal fluctuations has already been reported in the literature.[46] In our simulations, based in periodic models, stresses due to free edges do not naturally occur, but it is interesting to notice how our uniform compressive strain of -0.05 yields results comparable to those simulations. To introduce a finite temperature in our simulations we use *ab initio* molecular dynamics to follow the trajectories of carbon atoms in a 4×4 unit cell in equilibrium with a Nose-Hoover thermostat at $T = 300$ K. Starting out from an equilibrium distribution, the graphene layer is allowed to evolve in the canonical ensemble for $\tau_0 = 1$ ps using a $\Delta t = 0.5$ fs step to integrate the equations of motion. As before, the same two statistical indicators, $\bar{c}$ and c_M, are computed by averaging over all the configurations reached inside the time interval τ_0 (the shape of the layer at a time chosen at random, $t = 260$ fs, is shown in the upper panel of Fig. 4). Table IV shows values for three strains on the unit cell: $\epsilon = 0, -0.03$, and -0.05. The last two strains
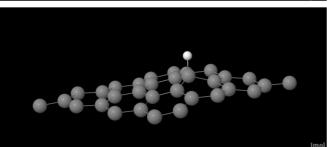

FIG. 4. (Color online) Upper panel: Snapshot configuration for a graphene layer subject to vibrations at $T = 300$ K (an arbitrary time, $t = 260$ fs, has been chosen). Lower panel: Equilibrium positions on the graphene layer upon hydrogen adsorption.

TABLE IV. Average, $\bar{c}$ (Å), and maximum, c_M (Å), corrugations in a graphene layer subject to an external thermal bath ($T = 300$ K), the adsorption of a light atom (H), or related to the intrinsic instability due to its 2D character (mode AZ in Ref. 2).

Case	$n \times n$	$\epsilon = 0.00$		$\epsilon = -0.03$		$\epsilon = -0.05$	
		$\bar{c}$	c_M	$\bar{c}$	c_M	$\bar{c}$	c_M
$T = 300$ K	4×4	0.069	0.572	0.153	1.280	0.309	2.349
H	4×4	0.041	0.432	0.168	1.061	0.310	1.580
Phonon ZA	8×2	0.000	0.000	0.662	2.034	0.917	2.807

correspond to stresses of $\sigma_{xx} = \sigma_{yy} = -0.94$ eV/Å² and -1.69 eV/Å², respectively. The case $\epsilon = 0$ allows a double check by comparing with the experimental Debye-Waller factor determined from low-energy electron diffraction on graphite (0001):[47] 0.053 Å to be compared with a value of 0.069 Å as derived from the simulation. Even for the small strain values considered here, the nonlinear growth of corrugations vs the external strain is clear.

C. Adsorption of a light impurity

A further source for corrugations at the atomic level is the presence of defects. For the sake of simplicity, we consider the adsorption of a light element (hydrogen atom), which is known to originate a static distortion in the lattice that depends on the coverage θ and extends as a long-range elastic perturbation.[27] For $\theta = \frac{1}{16}$, a value where the interaction between periodic images of the adsorbate is already low and can be representative of the behavior for the isolated impurity, both the averaged and the maximum corrugation take values fairly similar to the ones obtained by heating the layer to $T = 300$ K, except perhaps for the value of c_M, that systematically takes lower values for the thermal case (Table III). The corrugations studied here lead to partial sp^3 hybridization of the carbon orbitals, enhancing the spin-orbit coupling.[48]

IV. CONCLUSIONS

We find that averaged atomic corrugations of ≈ 0.05 Å, and maximum corrugation values of ≈ 0.5 Å are easily obtained under realistic conditions of cleanness and temperature on graphene layers. Corrugations due to thermal vibrations of atoms at room temperature make a similar effect to the adsorption of a light atom (H) with a moderately small coverage ($\theta = 1/16$). An external compressive stress increases corrugations in a nonlinear way. Due to the flexural mode, the graphene layer becomes intrinsically unstable and shows a value for the maximum corrugation under compressive stress three or four times larger than values attained at $T \leqslant 300$ K or because of the adsorption of impurities. Upon a 4% contraction, the LO and TO modes increase their frequencies by about 20%, while the main elastic constant affected is c_{12}, which is approximately halved.[49,50] On the other hand, the frequencies of the ZA and ZO modes are reduced. These modes induce an effective sp^3 coordination in the lattice, and their softening under strain leads to an enhancement of the intrinsic spin-orbit coupling,[48] opening a way to observe topological

insulator features in graphene.[51] Finally, these simulations have been useful to obtain the elastic constants needed to construct an analytical model of freestanding membranes based in elasticity theory.[23] Such a simple analytical model yields negative Grüneisen parameters related to the bending modes and a simple explanation for the negative thermal expansion coefficient of graphene.

[1] A. H. Castro Neto, F. Guinea, N. M. R. Peres, K. S. Novoselov, and A. K. Geim, Rev. Mod. Phys. **81**, 109 (2009).

[2] C. Lee, X. Wei, J. W. Kysar, and J. Hone, Science **321**, 385 (2008).

[3] P. L. de Andres, R. Ramirez, and J. A. Verges, Phys. Rev. B **77**, 045403 (2008).

[4] N. Abedpour, R. Asgari, and F. Guinea, Phys. Rev. B **84**, 115437 (2011).

[5] C. Si, W. Duan, Z. Liu, and F. Liu, arXiv:1210.8372.

[6] A. Fasolino, J. H. Los, and M. I. Katsnelson, Nature Mater. **6**, 858 (2007).

[7] P. San-Jose, J. González, and F. Guinea, Phys. Rev. Lett. **106**, 045502 (2011).

[8] W. Bao, F. Miao, Z. Chen, H. Zhang, W. Jang, C. Dames, and C. Lau, Nat. Nanotechnol. **4**, 562 (2009).

[9] T. Mashoff, M. Pratzer, V. Geringer, T. J. Echtermeyer, M. C. Lemme, M. Liebmann, and M. Morgenstern, Nano Lett. **10**, 461 (2010).

[10] M. I. Katsnelson, *Graphene: Carbon in Two Dimensions* (Cambridge University Press, Cambridge, UK, 2012).

[11] N. Mounet and N. Marzari, Phys. Rev. B **71**, 205214 (2005).

[12] K. V. Zakharchenko, M. I. Katsnelson, and A. Fasolino, Phys. Rev. Lett. **102**, 046808 (2009).

[13] L. D. Landau and E. M. Lifshitz, *Statistical Mechanics*, Vol. I (Pergamon Press, Oxford, 1976).

[14] D. R. Nelson and L. Peliti, J. Phys. France **48**, 1085 (1987).

[15] J. A. Aronovitz and T. C. Lubensky, Phys. Rev. Lett. **60**, 2634 (1988).

[16] P. Le Doussal and L. Radzihovsky, Phys. Rev. Lett. **69**, 1209 (1992).

[17] D. W. Boukhvalov, M. I. Katsnelson, and A. I. Lichtenstein, Phys. Rev. B **77**, 035427 (2008).

[18] S. Viola Kusminskiy, D. K. Campbell, A. H. Castro Neto, and F. Guinea, Phys. Rev. B **83**, 165405 (2011).

[19] P. Hohenberg and W. Kohn, Phys. Rev. **136**, B864 (1964).

[20] W. Kohn and L. J. Sham, Phys. Rev. **140**, A1133 (1965).

[21] D. Sánchez-Portal, E. Artacho, J. M. Soler, A. Rubio, and P. Ordejón, Phys. Rev. B **59**, 12678 (1999).

[22] Y.-W. Son, M. L. Cohen, and S. G. Louie, Phys. Rev. Lett. **97**, 216803 (2006).

[23] P. L. de Andres, F. Guinea, and M. I. Katsnelson, Phys. Rev. B **86**, 144103 (2012).

[24] M.-H. Lee, Ph.D. thesis, The University of Cambridge, 1996.

[25] J. S. Lin, A. Qteish, M. C. Payne, and V. Heine, Phys. Rev. B **47**, 4174 (1993).

[26] D. M. Ceperley and B. J. Alder, Phys. Rev. Lett. **45**, 566 (1980).

[27] P. L. de Andres and J. A. Verges, Appl. Phys. Lett. **93**, 171915 (2008).

[28] S. Clark, M. D. Segall, C. Pickard, P. Hasnip, M. J. Probert, K. Refson, and M. C. Payne, Z. fuer Kristallographie **220**, 567 (2005).

[29] Materials Studio–CASTEP 6.0, 2012; http://www.accelrys.com.

[30] V. B. Deyirmenjian, V. Heine, M. C. Payne, V. Milman, R. M. Lynden-Bell, and M. W. Finnis, Phys. Rev. B **52**, 15191 (1995).

[31] S. Baroni, S. de Gironcoli, A. Dal Corso, and P. Giannozzi, Rev. Mod. Phys. **73**, 515 (2001).

[32] O. L. Blakslee, D. G. Proctor, E. J. Seldin, G. B. Spence, and T. Weng, J. Appl. Phys. **41**, 3373 (1970).

[33] A. Bosak, M. Krisch, M. Mohr, J. Maultzsch, and C. Thomsen, Phys. Rev. B **75**, 153408 (2007).

[34] G. Savini, Y. Dappe, S. Öerg, J.-C. Charlier, M. Katsnelson, and A. Fasolino, Carbon **49**, 62 (2011).

[35] K. H. Michel and B. Verberck, Phys. Rev. B **78**, 085424 (2008).

[36] L. D. Landau and E. M. Lifshitz, *Theory of Elasticity* (Pergamon Press, Oxford, 1976).

[37] R. Saito, G. Dresselhaus, and S. Dresselhaus, *Physical Properties of Carbon Nanotubes* (Imperial College Press, London, 1998).

[38] F. Liu, P. Ming, and J. Li, Phys. Rev. B **76**, 064120 (2007).

[39] Y. Zhang and F. Liu, Appl. Phys. Lett. **99**, 241908 (2011).

[40] C. A. Marianetti and H. G. Yevick, Phys. Rev. Lett. **105**, 245502 (2010).

[41] L. J. Karssemeijer and A. Fasolino, Surf. Sci. **605**, 1611 (2011).

[42] M. Pozzo, D. Alfè, P. Lacovig, P. Hofmann, S. Lizzit, and A. Baraldi, Phys. Rev. Lett. **106**, 135501 (2011).

[43] J. H. Strait, H. Wang, S. Shivaraman, V. Shields, M. Spencer, and F. Rana, Nano Lett. **11**, 4902 (2011).

[44] N. M. Gabor, J. C. W. Song, Q. Ma, N. L. Nair, T. Taychatanapat, K. Watanabe, T. Taniguchi, L. S. Levitov, and P. Jarillo-Herrero, Science **334**, 648 (2011).

[45] H. Ochoa, V. I. Falko, A. H. Castro Neto, and F. Guinea, arXiv:1209.4382.

[46] B. Huang, M. Liu, N. Su, J. Wu, W. Duan, B.-l. Gu, and F. Liu, Phys. Rev. Lett. **102**, 166404 (2009).

[47] N. J. Wu and A. Ignatiev, Phys. Rev. B **25**, 2983 (1982).

[48] A. H. Castro Neto and F. Guinea, Phys. Rev. Lett. **103**, 026804 (2009).

[49] A. Politano, A. R. Marino, and G. Chiarello, J. Phys.: Condens. Matter **24**, 104025 (2012).

[50] E. Cadelano and L. Colombo, Phys. Rev. B **85**, 245434 (2012).

[51] C. L. Kane and E. J. Mele, Phys. Rev. Lett. **95**, 226801 (2005).

[52] A. A. Ahmadieh and H. A. Rafizadeh, Phys. Rev. B **7**, 4527 (1973).